Carbohydrate Polymers 223 (2019) 115050

Contents lists available at ScienceDirect

Carbohydrate Polymers

journal homepage: www.elsevier.com/locate/carbpol

Thermally-induced cellulose nanofibril films with near-complete ultraviolet-blocking and improved water resistance

Weisheng Yang[a,b], Ying Gao[a], Chu Zuo[a], Yulin Deng[b,*], Hongqi Dai[a,*]

[a] Jiangsu Co-innovation Center for Efficient Processing and Utilization of Forestry Resources, Nanjing Forestry University, Nanjing, Jiangsu, 210037, China
[b] School of Chemical & Biomolecular Engineering and Renewable Bioproducts Institute, Georgia Institute of Technology, Atlanta, GA, 30318, USA

ARTICLE INFO

Keywords:
Thermal treatment
Cellulose nanofibril films
UV protection
Water resistance
Transparency

ABSTRACT

In recent years, ultraviolet (UV) protection films made from cellulose nanofibril (CNF) have drawn significant attention, owing to its high transparency, high mechanical strength and relatively high thermostability. Generally, CNF films had poor UV-shielding performance, and required UV absorbent to enhance their UV-shielding ability. Herein, a simple thermal treatment is proposed to directly improve the UV blocking properties of CNF films without incorporating UV absorbent. After thermal treatment at 160 °C, the CNF films exhibited a near-complete UV blocking ability. In particular, they exhibited full absorption of ultraviolet A (UVA) and ultraviolet B (UVB), and also showed a high visible light transmittance of 72%. In addition, the UV-shielding films performed stable UV-blocking when exposed to UV irradiation. Simultaneously, the hornification induced by thermal treatment endowed an improved hydrophobicity for CNF films. However, the tensile strength of the CNF films decreased from 133 MPa to 81 MPa after thermal treatment at 160 °C.

1. Introduction

Excessive exposure to sunlight can cause discoloration of dyes and pigments, yellowing of plastics and papers, sunburn or cancer in human skin, and other problems (Berneburg, Plettenberg, & Krutmann, 2000; Mackie, Elwood, & Hawk, 1987; Yousif & Haddad, 2013; Zayat, Garcia-Parejo, & Levy, 2007). This phenomenon arises from the ultraviolet (UV) wavelength portion of the spectrum of sunlight (Hattori, Ide, & Sano, 2014; Piccirillo et al., 2014). As the stratospheric ozone content in the atmosphere decreases, UV radiation from the solar spectrum is producing striking and ubiquitous detrimental effects on human health and other biological systems (Kerr & McElroy, 1993; Williamson, Neale, Grad, De Lange, & Hargreaves, 2001). Hence, in recent years, the development of high-efficiency UV-shielding products such as sunblock creams, sunglasses, hats, window protectors, arm protectors, and cloth has attracted significant attention from researchers.

Petroleum-based polymer matrices have been widely applied in UV-shielding materials (Tang, Cheng, Pang, Ma, & Xing, 2006; Tu et al., 2010; Xing, Ruch, Dubois, Wu, & Wang, 2017). However, such materials, as used in UV-protection products for specific purposes, are high cost and contain non-biodegradable substances. During the treatment of petroleum-based polymer wastes, large amounts of toxic and harmful substances are generated, which can cause serious damage to the environment. Hence, with increasing concern regarding environmental issues and the overexploitation of fossil resources, biodegradable cellulose-based materials have been developed to replace traditional petroleum-based polymer matrices. Cellulose nanofibrils (CNF) can be used to construct high-performance structural materials and functional composites, that exhibit many desirable properties, such as low cost, non-toxicity, biocompatibility, high mechanical strength, good optical properties, good thermostability, and low thermal expansion (Huang et al., 2013; Khalil, Bhat, & Yusra, 2012; Klemm et al., 2011). Hence, CNF, as an ideal building block, has been used for the fabrication of biodegradable, eco-friendly UV-shielding materials. Furthermore, CNF-based UV protection films exhibit great suitability for practical applications, such as clean windows, contact lens, and car windshields.

General approaches to achieving high UV protection have mainly relied on the incorporation of a UV absorber in the CNF films. For example, photoactive materials such as benzophenone, diisocyanate, epoxidized soybean oil, $Eu(TTA)_3(H_2O)_2$, and p-aminobenzoic acid have been chemically grafted onto CNF or cellulose nanocrystal (CNC) surfaces to improve UV blocking ability (Niu et al., 2018; Sirviö, Visanko, Heiskanen, & Liimatainen, 2016; Zhang et al., 2017). However, during the chemical grafting reactions, a large number of harmful chemicals are used, which is contrary to the requirements of "green chemistry". In addition, some organic or inorganic UV absorbents, such as ZnO, carbon dots, lignin, aramid nanofibers, and colored metal ions have been directly incorporated into CNF films through simple physical

* Corresponding authors.
E-mail addresses: yulin.deng@rbi.gatech.edu (Y. Deng), hgdhq@njfu.edu.cn (H. Dai).

https://doi.org/10.1016/j.carbpol.2019.115050
Received 21 March 2019; Received in revised form 2 July 2019; Accepted 2 July 2019
Available online 08 July 2019
0144-8617/

blending (Feng et al., 2017; Jiang et al., 2015; Luo et al., 2019; Wang et al., 2018; Yang, Wang, Gogoi, Bian, & Dai, 2019). For these studies, the incorporation of a second or third component is necessary for improving the UV blocking ability of the CNF films.

Thus, a simple and green thermal treatment technology is proposed herein, for preparing CNF films with near-complete UV-blocking properties and improved water resistant. The discoloration induced by a simple thermal treatment provides enhanced UV-shielding ability for the CNF films, which do not need a complicated modification process or additional UV absorbents. This idea is inspired by the yellow discoloration and hornification of paper fibers during thermal treatment (Hubbe, Venditti, & Rojas, 2007; Luo & Zhu, 2011). For fibrous materials, yellow discoloration and hornification will affect the appearance of the paper and limit the recycling and reuse of the fibers (McKinney, 1994). However, these phenomena bring new opportunities to CNF materials, as they provide enhanced UV-shielding properties and improved water resistance for CNF films. The hornification of CNF films induced by thermal treatment has been reported to enhance the barrier properties of CNF films (Österberg et al., 2013; Xia et al., 2018). However, we are not aware of publicly-available studies on the effects of thermal treatment on the UV-shielding performance of CNF films.

In this work, the UV-blocking CNF films were fabricated by a thermal treatment (Fig. 1). This study investigated the effects of the thermal treatment temperature on the visual appearances, visible light transmittance, UV-blocking, water resistance, thermal stability, and mechanical properties of the CNF films. The CNF films with near-complete UV-blocking properties and improved water resistance properties provide promising candidates for transparent UV-shielding materials to be applied in, e.g., clean windows, contact lenses, or car windshields.

2. Experiment and methods

2.1. Materials

TEMPO-oxidized cellulose nanofibril (TOCN) has been produced in previous studies (Isogai, Saito, & Fukuzumi, 2011; Yang, Jiao, Min, Liu, & Dai, 2017). The TOCN used in this study has a surface carboxylate content of 1.633 mmol/g, with a diameter of 6–8 nm (Figs. S1 and S2). The TOCN used in this study mainly consists of glucose (73.53%), xylose (14.19%), and small amounts of lignin (0.52%), as shown in Table S1.

2.2. Preparation of TOCN films

The TOCN films were prepared using a solution-casting method. A TOCN aqueous suspension was diluted to 0.5 wt% concentration by the addition of deionized water, and was stirred overnight to form a uniform aqueous suspension. The obtained 0.5 wt% TOCN dispersion was poured into a polystyrene Petri dish and dried at room temperature (25 °C) for 3 days, until the water completely evaporated and TOCN films were formed. The grammage of the films was approximately 30 g m^{-2}. The resultant films were then heated in an oven for 3 h at different temperatures (140 °C, 150 °C, 160 °C, and 170 °C) denoted as T140, T150, T160, and T170, respectively. The dried films, with thicknesses of 22–25 μm, were placed at 23 °C and 50% RH for 24 h to balance the moisture content.

2.3. Characterization

A Fourier-transform infrared spectroscopy (FTIR) spectrometer (VERTEX 80 V, Bruker, Germany) with a universal attenuated total-reflection (ATR) probe was used to analyze the TOCN film samples. X-ray diffraction patterns of the TOCN film samples were obtained using an X-ray diffractometer (Ultima IV, Rigaku, Japan) equipped with Cu-K_α radiation (λ =15.4 Å) in the range of 5–40° at a scan speed of 4°/min. All film samples were dried in a vacuum oven at 40 °C for 24 h to remove moisture before measurements. The crystallinity index (CrI, %) was calculated using Eq. (1):

$$CrI\,(\%) = \frac{I_{200} - I_{am}}{I_{200}} \times 100 \quad (1)$$

Here, I_{200} is the maximum intensity of the principal peak, and I_{am} is the intensity of diffraction attributed to amorphous cellulose (Segal, Creely, Martin, & Conrad, 1959). An Xrite i1 Pro2 spectrophotometer was utilized to analyze the chromaticity of the film samples. Currently, the most complete color space for describing the visible colors for the human eye is CIELAB, as specified by the International Commission on Illumination (CIE). The CIELAB hue cube consists of three components related to color: luminosity (L), a, and b. L represents the lightness of the color, where a low number (0–50) indicates darkness and a high

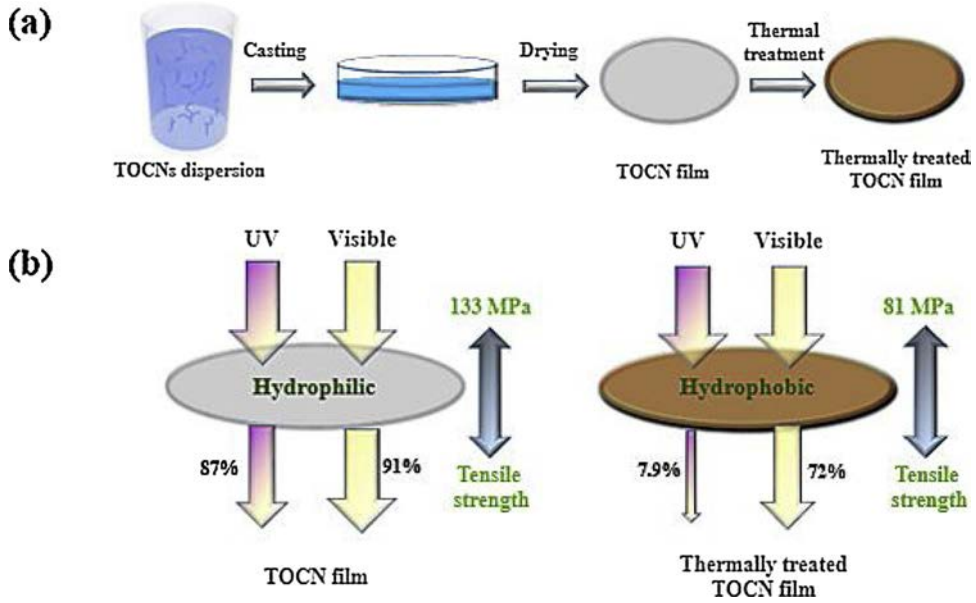

Fig. 1. (a) Schematic illustration of the fabrication of TOCN UV-blocking films, (b) Schematic describing of the UV-filtering and hydrophobicity of the thermally treated TOCN films.

number (51–100) refers to lightness. The value range of a and b is from +127 to −128, where a indicates the difference between green ($-a$) and red ($+a$), and b indicates the difference between yellow ($+b$) and blue ($-b$). Scanning electron microscopy (SEM) (Quanta-200, FEI, USA) was used to analyze the cross-sectional structure of the TOCN films. In addition, the thicknesses of the film samples were calculated according to the cross-sectional images of the TOCN films (Fig. S4). The UV-blocking properties of the TOCN film samples were investigated by measuring their absorbance and total transmittance using a UV–vis (VIS)/near infrared (NIR) spectrophotometer (Lambda 950, PerkinElmer, USA) with a wavelength range from 200 nm to 1100 nm. A wavelength of 555 nm was used for a determination of film transparency in the visible region, as it is the most sensitive wavelength for humans (Sirviö et al., 2016). The T(UVA) and T(UVB) of the TOCN film samples were calculated using Eqs. (2) and (3):

$$T(\mathrm{UVA}) = \frac{\int_{320}^{400} T_\lambda \times d\lambda}{\int_{320}^{400} d\lambda} \quad (2)$$

$$T(\mathrm{UVB}) = \frac{\int_{280}^{320} T_\lambda \times d\lambda}{\int_{280}^{320} d\lambda} \quad (3)$$

In the above, T_λ is the transmittance of the TOCN film samples of the light at wavelength λ. The absorption coefficients were calculated according to Beer-Lambert's law and Debye-Scherrer (Tauc's plot), to find the band gaps from the absorption data. The thermal stability of the TOCN film samples was measured using a thermogravimetric analyzer (PerkinElmer, Inc., Waltham, MA). Samples of approximately 5 mg were heated from 30 to 600 °C with a heating rate of 10 °C/min under a high purity nitrogen flow of 20 mL/min. The mechanical properties of the TOCN films were investigated using a tensile tester (H25KT, Tinius Olsen, USA) with a 500 N load cell at 1 mm/min, according to ASTM D638-03. The specimens have a typical size of 5 mm in width and 40 mm in length, and five measurements were carried out for each specimen. The water absorption ratio was measured using ASTM D570. The films were soaked in deionized water for 3 h. Then, the wet films were picked up, and excess water was removed by blotting paper. The contact angle of a 4 μL water droplet on the film sample surfaces was measured using a contact angle analyzer (Attention Theta, Biolin Scienfic, Inc. Stockholm, Sweden).

3. Result and discussion

3.1. Structures of TOCN films

In this study, a thermal treatment was utilized to directly improve the UV-blocking properties of transparent TOCN films, without incorporating UV absorbent. The visual appearances of the film samples are shown in Fig. 2. All of the film samples showed high transparency, and the printed patterns under the films could be clearly seen by human eyes. It was also observed that the thermal treatment could induce yellow or brown discoloration for the TOCN films (Takaichi, Saito, Tanaka, & Isogai, 2014; Xia et al., 2018; Yagyu, Saito, Isogai, Koga, & Nogi, 2015). Previous research showed that interfibrillar hemiacetal linkages are probably formed between the hydroxyl groups and C6-aldehydes present on the surfaces of TOCN during thermal treatment, which induces significant discoloration (Isogai et al., 2011; Shinoda, Saito, Okita, & Isogai, 2012). Empirical methods for detecting C6-aldehydes were investigated using the UV spectra of the TOCN films (Fig. S3). It is possible that the UV absorption peaks at approximately 260 nm can be ascribed to the C6-aldehydes (Takaichi et al., 2014). The small amount of residual lignin (0.52%) also induced a weak discoloration phenomenon. Commonly, after a bleaching processes, the conjugate bonds (chromophoric group) in lignin were opened, and the color was removed. After the thermal treatment in the air, the opening double bond of the lignin came back together and became a conjugate bond, which induced the discoloration. Hence, small amounts of C6 aldehydes and the residual lignin in the TOCN have vital roles in the discoloration of the TOCN films after thermal treatment.

The chromaticity represented the color difference of the film samples, and was based on the visual physiology of the human eye. The chromaticity of the film samples was measured using an Xrite i1 Pro2 spectrophotometer. CIELAB was utilized to describe the visible colors for the human eye. The detailed CIELAB film samples are shown in Table 1. As the thermal treatment temperature increased, significant variations to the values of L, a, and b were observed between the film samples. As the thermal treatment temperature increased, the a and b values increased from −1.21 to 18.95 and from 1.18 to 46.79, respectively, indicating that the red and yellow colors of the TOCN films were getting deeper. In that regard, the yellow or brown discoloration for the TOCN films induced by thermal treatment was detectable by human eyes.

The FT-IR spectra of the film samples are shown in Fig. 3a. The absorption peak at 1600 cm^{-1} corresponds to the C=O stretching vibration of sodium carboxylates (Fujisawa, Saito, & Isogai, 2012; Shimizu, Fukuzumi, Saito, & Isogai, 2013). The peaks at 1415, 1029, and 900 cm^{-1} represent the typical structure of cellulose (Leung et al., 2011). The results suggest that the thermal treatment had a limited influence on the chemical structure of cellulose. As compared with the spectrum of the original TOCN film, the peak intensity of O—H stretching was decreased after thermal treatment, which is the result of the decrease of absorbed water content after thermal treatment (Li & Renneckar, 2011).

X-ray diffraction (XRD) was performed to analyze the impact of the thermal treatment on the crystalline structure of the TOCN films. Fig. 3b shows the XRD profile of the TOCN films. All of the film samples exhibited a typical cellulose I crystalline structure, with diffraction peaks at 14.6°,16.5°and 22.6°, respectively. The results indicated that the thermal treatment had a limited influence on the crystalline structure of the TOCN films. With a low treatment temperature (less than 160 °C), the crystallinity values of the TOCN film showed a slight changing which indicated a good stability. When the TOCN films were treated with a higher temperature of 170 °C, the crystallinity of TOCN films decreased from 75.46% to 71.99%, owing to the excessive decomposition of the TOCN films and destruction of the crystalline structure caused by the high temperatures.

3.2. UV protection properties

The UV–vis light transmittances of the film samples collected in the region of 200–1100 nm are presented in Fig. 4. As 555 nm is the most sensitive wavelength for humans, it was used as a reference to track the evolution of the optical properties of the film samples in the visible region (Sirviö et al., 2016). For intuitively depicting the UV-shielding performance of these TOCN films, the transmittance of ultraviolet A (UVA), ultraviolet B (UVB), i.e., (T(UVA) and T(UVB)), were respectively calculated using the equations reported previously (Table 2). Owing to dense packing or nanoscale dimensions, the TOCN films could effectively avoid light scattering, and exhibited high transparency in the visible region (400–1100 nm) (Fig. 4a). However, the original TOCN films had weak absorption at UV region (200–400 nm), which was the reason for the poor UV-shielding performance.

From Table 2, it can be seen that the original TOCN films had high optical transmittance, with 91.1%, 86.9%, and 71.5% for T(555 nm), T(UVA), and T(UVB), respectively. After the thermal treatment, the optical ban gap of the film samples decreased from 5.44 Ev to 3.06 Ev. The smaller optical band gap induced a wider light absorption range, and enhanced the UV-shielding performance. Hence, the transparency in all UV–vis spectra showed a considerable decline, and this trend got more severe with the increase of thermal treatment temperature. This phenomenon was attributed to the UV absorption becoming more

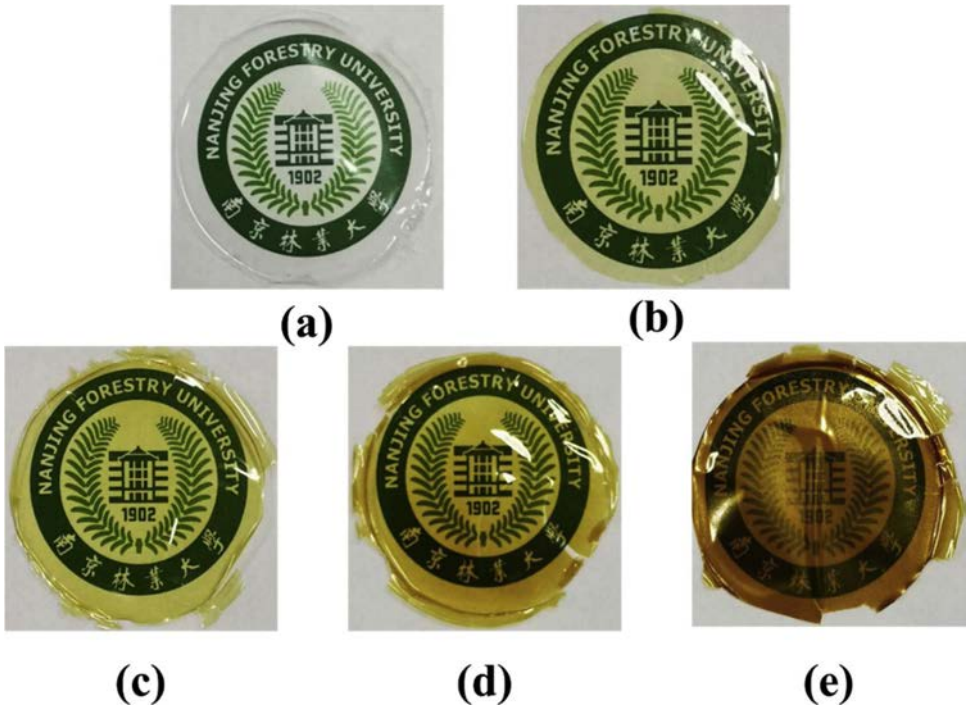

Fig. 2. The visual appearances of original TOCN film and thermally treated TOCN films (a) original, (b) 140 °C, (c) 150 °C, (d) 160 °C, (e) 170 °C.

Table 1
CIELAB of original TOCN film and thermally treated TOCN films.

Sample	*L*	*a*	*b*
Original	86.84	−1.21	1.18
T140	77.53	2.64	32.54
T150	71.74	7.38	45.94
T160	69.07	8.42	45.54
T170	40.80	18.95	46.79

intense with the forming of interfibrillar hemiacetal, the forming of the conjugate bond in the residual lignin, and the deepening red and yellow color. Previous research had indicated that the interfibrillar hemiacetal and lignin have certain UV absorption abilities (Takaichi et al., 2014; Wang et al., 2018). Some researchers have also indicated that color is one of the most influential variables on the protection against UV radiation (Gabrijelčič, Urbas, Sluga, & Dimitrovski, 2009; Riva, Algaba, Pepió, & Prieto, 2009). UV has a very short wavelength that is easily absorbed by materials that exhibit absorption in the visible part of the spectrum, as indicated by the red and yellow colors. As the CIELAB values show, as the thermal treatment temperature increased, the red and yellow colors of the TOCN films were getting deeper. Hence, the thermal treatment was excepted to endow enhanced UV-shielding performance for the TOCN films. The TOCN film treated with 160 °C exhibited over 92% absorption of UVA and full UVB absorption, and simultaneously maintained approximately 72% transparency for visible light. When the thermal treatment temperature reached 170 °C, the T(555 nm), T(UVA), and T(UVB) dramatically decreased to 37.3%, 0.4%, and 0%, respectively. Although the TOCN film treated with 170 °C exhibited almost complete absorption of UVA and UVB, its visible light transmittance was only 37.3%. The low visible light transparency limited its application, e.g., in clean windows, contact lenses, and car windshields.

This study also investigated the effect of the UV irradiation on UV-shielding stability. The film samples were irradiated using a UV xenon lamp (wavelength of 254 nm) for 12 h. The UV–vis transmission curves of the film samples before and after UV irradiation are shown in Fig. 4b. The results showed that the transmittance of the original TOCN films (T(555 nm), T(UVA), and T(UVB)) exhibited a certain stability under long-time UV irradiation. Significantly, the UV-shielding of TOCN film treatment under 170 °C remained relatively stable under UV irradiation. The results showed a slight increase of 3.2% and 0.4% in UVA and UVB transmittance after UV irradiation.

3.3. Mechanical properties

The mechanical properties of TOCN films are essential for their practical applications. The stress-strain curves of the TOCN films before

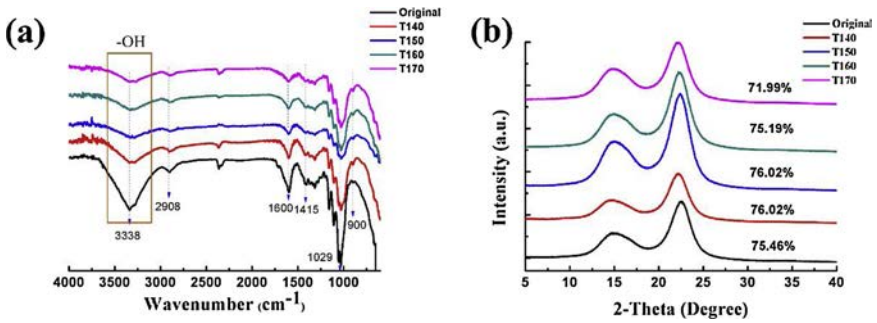

Fig. 3. (a) FT-IR spectra of original TOCN film and thermally treated TOCN films. (b) XRD patterns of original TOCN film and thermally treated TOCN films.

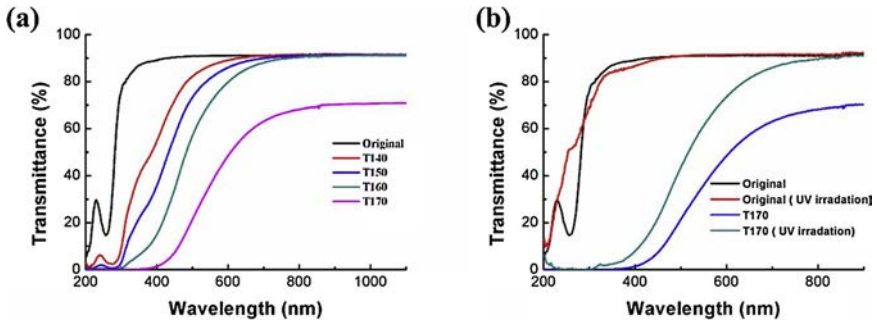

Fig. 4. (a) UV–vis transmission curves of original TOCN film and thermally treated TOCN films. (b) Effects of UV irradiation for 12 h of film samples on their light transmittance behavior.

Table 2
The transmittance of ultraviolet A, ultraviolet B, and visible light of original TOCN film and thermally treated TOCN films.

Sample	Thickness (μm)	Optical band gap (eV)	T_a(555 nm) (%)	T_b(555 nm) (%)	T_a(UVA) (%)	T_b(UVA) (%)	T_a(UVB) (%)	T_b(UVB) (%)
Original	17.2	5.44	91.1	91.1	86.9	86.9	71.5	71.5
T140	15.4	4.90	87.0	–	41.9	–	11.5	–
T150	16.9	4.63	81.9	–	24.1	–	4.6	–
T160	14.5	3.76	72.0	–	7.9	–	0.9	–
T170	14.6	3.06	37.3	62.4	0.4	3.6	0	0.4

T_a is the transmittance of film samples without UV irradiation. T_b is the transmittance of film samples after UV irradiation (the wavelength of 254 nm) for 12 h.

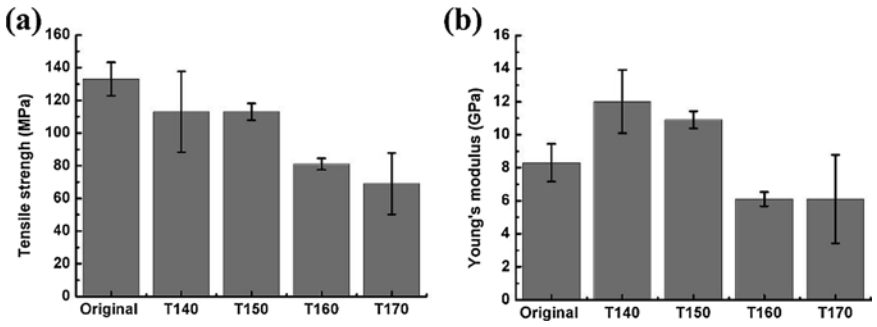

Fig. 5. Tensile strength (a), Young's modulus (b) of original TOCN film and thermally treated TOCN films.

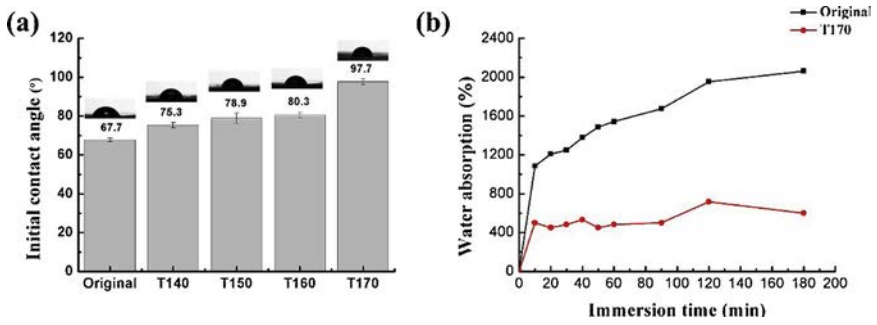

Fig. 6. Water contact angels (a) time-dependent water absorption (b) of original TOCN film and thermally treated TOCN films.

and after thermal treatment are provided in Fig. S6, and typical mechanical properties of the film samples are shown in Fig. 5. A high tensile strength of 133 MPa and Young's modulus of 8.3 GPa was observed for the original TOCN films, owing to the compactly interfibrillar hydrogen bond network (Benítez, Torres-Rendon, Poutanen, & Walther, 2013). After the thermal treatment, the TOCN films should show a better tensile strength, owing to the formation of irreversible hydrogen bonds. However, with increasing treatment temperature, the tensile strength of the film samples tended to decrease, as shown in Fig. 5a. As for the TOCN films treated at 170 °C for 3 h, the tensile strength reduced to 69 MPa, which was lower than the original TOCN films. These results implied that the treatment temperature is high enough to cause a decrease in the degree of polymerization of TOCN, and to cause the TOCN films to become increasingly brittle (Vieira & Rocha, 2007). As shown in Fig. 3b, with the increased treatment temperature, the Young's modulus of the TOCN film samples first increased, and then decreased. In general, high temperature (140–170 °C) thermal treatment caused significant damage to the mechanical properties of the TOCN films. Although the thermal treatment resulted in a decrease in the mechanical properties, the TOCN films still remained at a relatively high tensile strength and Young's modulus.

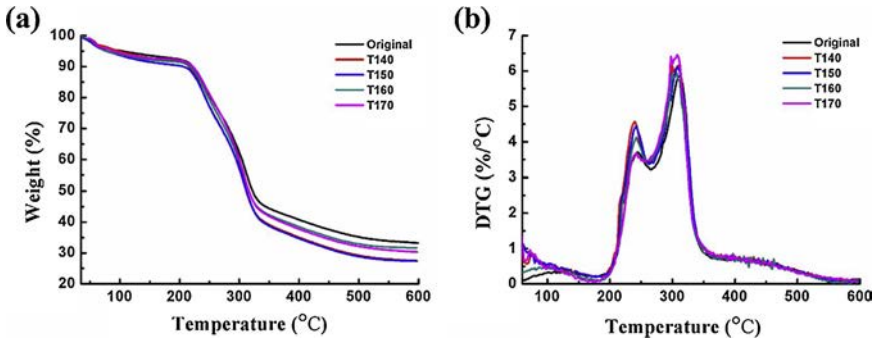

Fig. 7. TG (a) and DTG (b) curves of original TOCN film and thermally treated TOCN films.

3.4. Water-resistance properties

The hydrophilic nature of the TOCN materials could cause serious problems in practical applications, especially under humid conditions (Belbekhouche et al., 2011; Benítez et al., 2013). With the thermal treatment temperature increased, the moisture content of the TOCN films showed an evidently declining trend (Fig. S5). As shown in Fig. 6a, the original TOCN films exhibited relatively high hydrophilicity, with a low initial contact angle of 67.7°. The hydrophilicity could be attributed to the large amounts of hydrophilic groups including hydroxyl and carboxylate groups, exposed onto the TOCN surfaces (Shimizu, Saito, & Isogai, 2016; Yang, Bian et al., 2017). Herein, thermal treatment was utilized to improve the water resistance of the TOCN materials. As shown in Fig. 6a, an evident improvement of the contact angle could be observed after the thermal treatment. After thermal treatment at 170 °C, the contact angles of water droplets increased from 67.7° to 97.7°, indicating an increase of the water resistance of the TOCN films. The improvement of the water resistance was also evidenced by the decrease of the water absorption. As shown in Fig. 6b, as compared with the original TOCN films, the water absorption of the TOCN films after thermal treatment at 170 °C decreased from 2063% to 600%. These results could be ascribed to the hornification of TOCN caused by thermal treatment (Chen et al., 2011; Österberg et al., 2013; Xia et al., 2018), which reduced the swelling of the films and increased the hydrophobicity. Hornification of cellulose fibers is frequently associated with formation of irreversible hydrogen bonding upon a thermal treatment process (Diniz, Gil, & Castro, 2004). Thus, the results suggest that thermal treatment also plays a crucial role in the improvement of the water resistance of TOCN films.

3.5. Thermal stability

The thermogravimetric (TG) and derivative curves (DTG) of the film samples are shown in Fig. 7. Three degradation phases were observed during the entire thermal transition of the film samples. The slight weight loss under 200 °C was caused by the evaporation of residual water in the films. The two subsequent major weight losses, from 100 to 600 °C, were attributed to the decomposition of sodium carboxylates in the range from 200 to 270 °C, and to the decomposition of cellulose at 270–600 °C (Lavoine, Bras, Saito, & Isogai, 2016; Sun, Wu, Ren, & Lei, 2015). With the thermal treatment, the weight loss of the film samples still occurred in three main steps. However, the temperature at which the maximum rate of degradation occurred decreased after the thermal treatment, which was reasonable because of the degradation of the membrane during the thermal treatment. On the whole, the thermal stability of the TOCN films was slightly decreased after the thermal treatment, but it remained high enough for most practical applications.

4. Conclusions

In this study, a thermal treatment was proposed to prepare optical TOCN films with enhanced UV-blocking properties and improved water resistance. Thermal treatment induced yellow or brown discoloration for the TOCN films. The yellow or brown discoloration could primarily filter UV irradiation ranging from 200 to 400 nm, and maintained a high transparency for visible light. After thermal treatment at 160 °C for 3 h, the CNF films exhibited a near-complete UV blocking ability, especially full absorption of UVA and UVB, and a high visible light transmittance of 72%. The UV-shielding ability of the film samples was persistent when exposed to UV irradiation for a long time. TOCN films also became more hydrophobic after thermal treatment, which was beneficial for the film samples used under humid conditions. Although the mechanical properties and thermal stability of the TOCN films showed a decline after thermal treatment, they were still high enough for most practical applications.

Acknowledgements

This work was supported by the introduction of Advanced International Project of Forestry Science and Technology (Grant Number: 2015454), the National Natural Science Foundation of China (Grant Number: 31470599), the Doctorate Fellowship Foundation of Nanjing Forestry University. The authors also thank Linfei Ding, Jing Yang and Zhina Lian of Nanjing Forestry University for the SEM and HPLC measurements.

Appendix A. Supplementary data

Supplementary material related to this article can be found, in the online version, at doi:https://doi.org/10.1016/j.carbpol.2019.115050.

References

Belbekhouche, S., Bras, J., Siqueira, G., Chappey, C., Lebrun, L., Khelifi, B., et al. (2011). Water sorption behavior and gas barrier properties of cellulose whiskers and microfibrils films. *Carbohydrate Polymers, 83*, 1740–1748.

Benítez, A. J., Torres-Rendon, J., Poutanen, M., & Walther, A. (2013). Humidity and multiscale structure govern mechanical properties and deformation modes in films of native cellulose nanofibrils. *Biomacromolecules, 14*, 4497–4506.

Berneburg, M., Plettenberg, H., & Krutmann, J. (2000). Photoaging of human skin. *Photodermatology, Photoimmunology & Photomedicine, 16*, 239–244.

Chen, Y.-m., Wan, J.-q., Huang, M.-z., Ma, Y.-w., Wang, Y., Lv, H.-l., et al. (2011). Influence of drying temperature and duration on fiber properties of unbleached wheat straw pulp. *Carbohydrate Polymers, 85*, 759–764.

Diniz, J. F., Gil, M., & Castro, J. (2004). Hornification—its origin and interpretation in wood pulps. *Wood Science and Technology, 37*, 489–494.

Feng, X., Zhao, Y., Jiang, Y., Miao, M., Cao, S., & Fang, J. (2017). Use of carbon dots to enhance UV-blocking of transparent nanocellulose films. *Carbohydrate Polymers, 161*, 253–260.

Fujisawa, S., Saito, T., & Isogai, A. (2012). Nano-dispersion of TEMPO-oxidized cellulose/aliphatic amine salts in isopropyl alcohol. *Cellulose, 19*, 459–466.

Gabrijelčič, H., Urbas, R., Sluga, F., & Dimitrovski, K. (2009). Influence of fabric constructional parameters and thread colour on UV radiation protection. *Fibres and Textiles in Eastern Europe, 17*, 46–54.

Hattori, H., Ide, Y., & Sano, T. (2014). Microporous titanate nanofibers for highly efficient UV-protective transparent coating. *Journal of Materials Chemistry A, 2*, 16381–16388.

Huang, J., Zhu, H., Chen, Y., Preston, C., Rohrbach, K., Cumings, J., et al. (2013). Highly transparent and flexible nanopaper transistors. *ACS Nano, 7*, 2106–2113.

Hubbe, M. A., Venditti, R. A., & Rojas, O. J. (2007). What happens to cellulosic fibers during papermaking and recycling: A review. *BioResources, 2*, 739–788.
Isogai, A., Saito, T., & Fukuzumi, H. (2011). TEMPO-oxidized cellulose nanofibers. *Nanoscale, 3*, 71–85.
Jiang, Y., Song, Y., Miao, M., Cao, S., Feng, X., Fang, J., et al. (2015). Transparent nanocellulose hybrid films functionalized with ZnO nanostructures for UV-blocking. *Journal of Materials Chemistry C, 3*, 6717–6724.
Kerr, J., & McElroy, C. (1993). Evidence for large upward trends of ultraviolet-B radiation linked to ozone depletion. *Science, 262*, 1032–1034.
Khalil, H. A., Bhat, A., & Yusra, A. I. (2012). Green composites from sustainable cellulose nanofibrils: A review. *Carbohydrate Polymers, 87*, 963–979.
Klemm, D., Kramer, F., Moritz, S., Lindström, T., Ankerfors, M., Gray, D., et al. (2011). Nanocelluloses: A new family of nature-based materials. *Angewandte Chemie International Edition, 50*, 5438–5466.
Lavoine, N., Bras, J., Saito, T., & Isogai, A. (2016). Improvement of the thermal stability of tempo-oxidized cellulose nanofibrils by heat-induced conversion of ionic bonds to amide bonds. *Macromolecular Rapid Communications, 37*, 1033–1039.
Leung, A. C., Hrapovic, S., Lam, E., Liu, Y., Male, K. B., Mahmoud, K. A., et al. (2011). Characteristics and properties of carboxylated cellulose nanocrystals prepared from a novel one-step procedure. *Small, 7*, 302–305.
Li, Q., & Renneckar, S. (2011). Supramolecular structure characterization of molecularly thin cellulose I nanoparticles. *Biomacromolecules, 12*, 650–659.
Luo, J., Zhang, M., Yang, B., Liu, G., Tan, J., Nie, J., et al. (2019). A promising transparent and UV-shielding composite film prepared by aramid nanofibers and nanofibrillated cellulose. *Carbohydrate Polymers, 203*, 110–118.
Luo, X., & Zhu, J. (2011). Effects of drying-induced fiber hornification on enzymatic saccharification of lignocelluloses. *Enzyme and Microbial Technology, 48*, 92–99.
Mackie, R. M., Elwood, J., & Hawk, J. (1987). Links between exposure to ultraviolet radiation and skin cancer. *Journal of the Royal College of Physicians of London, 21*, 91–96.
McKinney, R. (1994). *Technology of paper recycling.* Berlin: Springer Science & Business Media.
Niu, X., Liu, Y., Fang, G., Huang, C., Rojas, O. J., & Pan, H. (2018). Highly transparent, strong, and flexible films with modified cellulose nanofiber bearing UV shielding property. *Biomacromolecules, 19*, 4565–4575.
Österberg, M., Vartiainen, J., Lucenius, J., Hippi, U., Seppälä, J., Serimaa, R., et al. (2013). A fast method to produce strong NFC films as a platform for barrier and functional materials. *ACS Applied Materials & Interfaces, 5*, 4640–4647.
Piccirillo, C., Rocha, C., Tobaldi, D., Pullar, R., Labrincha, J., Ferreira, M., et al. (2014). A hydroxyapatite–Fe_2O_3 based material of natural origin as an active sunscreen filter. *Journal of Materials Chemistry B, 2*, 5999–6009.
Riva, A. N., Algaba, I. S., Pepió, M., & Prieto, R. (2009). Modeling the effects of color on the UV protection provided by cotton woven fabrics dyed with azo dyestuffs. *Industrial & Engineering Chemistry Research, 48*, 9817–9822.
Segal, L., Creely, J., Martin, A., Jr., & Conrad, C. (1959). An empirical method for estimating the degree of crystallinity of native cellulose using the X-ray diffractometer. *Textile Research Journal, 29*, 786–794.
Shimizu, M., Fukuzumi, H., Saito, T., & Isogai, A. (2013). Preparation and characterization of TEMPO-oxidized cellulose nanofibrils with ammonium carboxylate groups. *International Journal of Biological Macromolecules, 59*, 99–104.
Shimizu, M., Saito, T., & Isogai, A. (2016). Water-resistant and high oxygen-barrier nanocellulose films with interfibrillar cross-linkages formed through multivalent metal ions. *Journal of Membrane Science, 500*, 1–7.
Shinoda, R., Saito, T., Okita, Y., & Isogai, A. (2012). Relationship between length and degree of polymerization of TEMPO-oxidized cellulose nanofibrils. *Biomacromolecules, 13*, 842–849.
Sirviö, J. A., Visanko, M., Heiskanen, J. P., & Liimatainen, H. (2016). UV-absorbing cellulose nanocrystals as functional reinforcing fillers in polymer nanocomposite films. *Journal of Materials Chemistry A, 4*, 6368–6375.
Sun, X., Wu, Q., Ren, S., & Lei, T. (2015). Comparison of highly transparent all-cellulose nanopaper prepared using sulfuric acid and TEMPO-mediated oxidation methods. *Cellulose, 22*, 1123–1133.
Takaichi, S., Saito, T., Tanaka, R., & Isogai, A. (2014). Improvement of nanodispersibility of oven-dried TEMPO-oxidized celluloses in water. *Cellulose, 21*, 4093–4103.
Tang, E., Cheng, G., Pang, X., Ma, X., & Xing, F. (2006). Synthesis of nano-ZnO/poly (methyl methacrylate) composite microsphere through emulsion polymerization and its UV-shielding property. *Colloid and Polymer Science, 284*, 422–428.
Tu, Y., Zhou, L., Jin, Y. Z., Gao, C., Ye, Z. Z., Yang, Y. F., et al. (2010). Transparent and flexible thin films of ZnO-polystyrene nanocomposite for UV-shielding applications. *Journal of Materials Chemistry, 20*, 1594–1599.
Vieira, M., & Rocha, S. (2007). Drying conditions influence on physical properties of recycled paper. *Chemical Engineering and Processing-Process Intensification, 46*, 955–963.
Wang, Q., Du, H., Zhang, F., Zhang, Y., Wu, M., Yu, G., et al. (2018). Flexible cellulose nanopaper with high wet tensile strength, high toughness and tunable ultraviolet blocking ability fabricated from tobacco stalk via a sustainable method. *Journal of Materials Chemistry A, 6*, 13021–13030.
Williamson, C. E., Neale, P. J., Grad, G., De Lange, H. J., & Hargreaves, B. R. (2001). Beneficial and detrimental effects of UV on aquatic organisms: Implications of spectral variation. *Ecological Applications, 11*, 1843–1857.
Xia, J., Zhang, Z., Liu, W., Li, V. C., Cao, Y., Zhang, W., et al. (2018). Highly transparent 100% cellulose nanofibril films with extremely high oxygen barriers in high relative humidity. *Cellulose, 25*, 4057–4066.
Xing, Q., Ruch, D., Dubois, P., Wu, L., & Wang, W.-J. (2017). Biodegradable and high-performance poly (butylene adipate-co-terephthalate)–lignin UV-blocking films. *ACS Sustainable Chemistry & Engineering, 5*, 10342–10351.
Yagyu, H., Saito, T., Isogai, A., Koga, H., & Nogi, M. (2015). Chemical modification of cellulose nanofibers for the production of highly thermal resistant and optically transparent nanopaper for paper devices. *ACS Applied Materials & Interfaces, 7*, 22012–22017.
Yang, W., Bian, H., Jiao, L., Wu, W., Deng, Y., & Dai, H. (2017). High wet-strength, thermally stable and transparent TEMPO-oxidized cellulose nanofibril film via cross-linking with poly-amide epichlorohydrin resin. *RSC Advances, 7*, 31567–31573.
Yang, W., Jiao, L., Min, D., Liu, Z., & Dai, H. (2017). Effects of preparation approaches on optical properties of self-assembled cellulose nanopapers. *RSC Advances, 7*, 10463–10468.
Yang, W., Wang, X., Gogoi, P., Bian, H., & Dai, H. (2019). Highly transparent and thermally stable cellulose nanofibril films functionalized with colored metal ions for ultraviolet blocking activities. *Carbohydrate Polymers, 213*, 10–16.
Yousif, E., & Haddad, R. (2013). Photodegradation and photostabilization of polymers, especially polystyrene. *SpringerPlus, 2*, 398–430.
Zayat, M., Garcia-Parejo, P., & Levy, D. (2007). Preventing UV-light damage of light sensitive materials using a highly protective UV-absorbing coating. *Chemical Society Reviews, 36*, 1270–1281.
Zhang, Z., Chang, H., Xue, B., Han, Q., Lü, X., Zhang, S., et al. (2017). New transparent flexible nanopaper as ultraviolet filter based on red emissive Eu (III) nanofibrillated cellulose. *Optical Materials, 73*, 747–753.